SELECTIVE EXCITATION: AN APPRAISAL OF MODULATED PULSES

Zenon Starčuk Jr.

Institute of Scientific Instruments
Czechoslovak Academy of Sciences
Královopolská 147, 612 64 Brno
Czechoslovakia

For the design of multipulse selective excitation sequences, a simple way of assessing the pulse demands and of calculating the excitation profiles corresponding to the separate echoes is often useful. The single prerequisite is a good knowledge of the performance of the pulses used. Much work has been done in this field in the recent few years, both in theory and practice. The description of pulse performance by excitation profiles being insufficient (1), more genuine properties have been found (2,3,4).

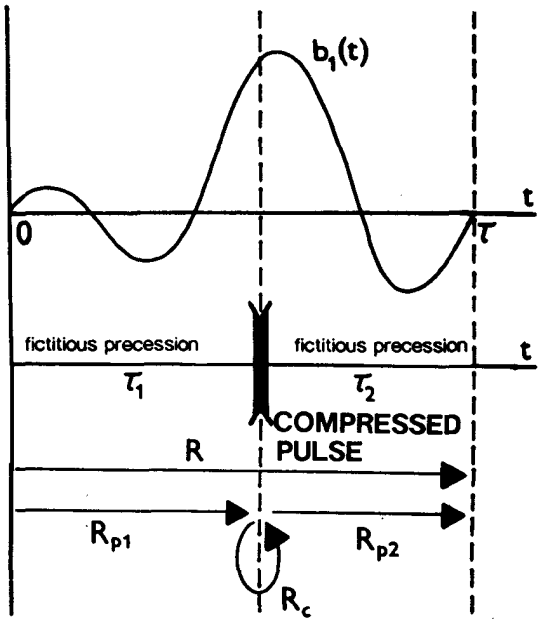

Fig. 1: Compressed pulse as a model of a real pulse.

Their list can be completed if the coherence transfer pathway (CTP) model (5) is applied consistently. The only problem- the temporal extension of the selective pulses - is circumvented easily by introducing a concept of **compressed pulses**. It is based on expressing the total pulse propagator R by means of a composition $R=R_{p2}.R_c.R_{p1}$ of two suitable free precession propagators R_{p1}, R_{p2} and a compressed pulse propagator R_c, as indicated in Fig. 1. In this way, all the substantial properties of the pulse get conceptually compressed into a single moment enclosed by two fictitious free precession intervals. This moment becomes the point of splitting the pathways, where each parent pathway excitation profile, treated as a function of position (r) and offset ($\nu = \nu_{cs} + \gamma B_0$), is multiplied by an appropriate **transition profile** C..= A..exp(iφ..). For an n-level system, n^2 complex, mutually interrelated transition profiles can be derived from the compressed pulse propagator R_c. These transition profiles as functions of the total offset ($\nu + \gamma$r.g) and the local B_1 intensity fully determine the effects of selectivity, separating them from the linear phase gradient evolution that can be described by k-trajectories of the individual pathways. By multiplying the appropriate transition profiles of the pulses used in the sequence, the excitation profile of any pathway, i.e. of any echo, can be found.

For **isolated spins 1/2** a simplified CTP model can be accepted, using only I_z, I_- coordinates and distinguishing two kinds of pathways: longitudinal (L) and transversal (T). Each pathway splitting (Fig. 2) gives rise to an L- and to two T-pathways, one of which (P) passes without phase inversion, while the phase of the other (I) is inverted prior to the profile multiplication. If the compressed pulse is described by a rotation matrix $R_{\beta,\alpha}(\vartheta)$ (6), the transition profiles are

$$C_{TP} = ((R_{xx}+R_{yy})+i(R_{yx}-R_{xy}))/2$$
$$C_{TI} = ((R_{xx}-R_{yy})+i(R_{yx}+R_{xy}))/2$$
$$C_{TL} = R_{xz}-iR_{xy}$$
$$C_{LT} = R_{xz}+iR_{yz} \quad = 2\,C_{LP} = 2\,C_{LI}$$
$$C_{LL} = R_{zz}.$$

Their mutual relations become more clearly visible, if three more fundamental profiles

$$Q = \cos\alpha.\sin(\vartheta/2),$$
$$\psi = -\pi/2+\arg(\cos(\vartheta/2)+ +i\sin\alpha.\sin(\vartheta/2)),$$

and β are chosen to express them:

$$A_{TP}=1-Q^2 \qquad \varphi_{TP} = 2\psi+\pi$$
$$A_{TI}= Q^2 \qquad \varphi_{TI} = 2\beta$$
$$A_{TL}=2Q\sqrt{(1-Q^2)} \qquad \varphi_{TL} = \psi - \beta$$
$$A_{LT}=2Q\sqrt{(1-Q^2)} \qquad \varphi_{LT} = \psi + \beta$$
$$A_{LL}=1-2Q^2 \qquad \varphi_{LL} = 0.$$

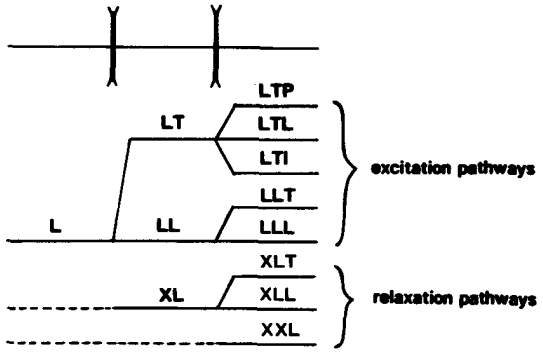

Fig. 2: New pathways created by pathway splitting and/or relaxation.

With this theoretical approach, various phase-cycling or gradient-pulse schemes for **pathway separation** can be found easily. Especially in designing the gradient spoiler pulses according to one of the principles depicted in Fig. 3, the possibility of substituting even more pulses by a single compressed pulse can be taken advantage of. For reference, also the correspondence of phase cycles and the transitions selected is summarized in Table 1.

The **transition profile of interest**, which can be optimized, depends on the type of the echo measured, the coding method, and the degree of separation of pathways: it is A_{LL} for population inversion, A_{LT} or C_{LT} for signal excitation, A_{TL} or C_{TL} for stimulated echo generation, A_{TI} or C_{TI} for refocusing. Other profiles can be decisive if superimposed echoes are measured (e.g. $\sqrt{A_{TI}}$ in CPMG sequences without pathway separation).

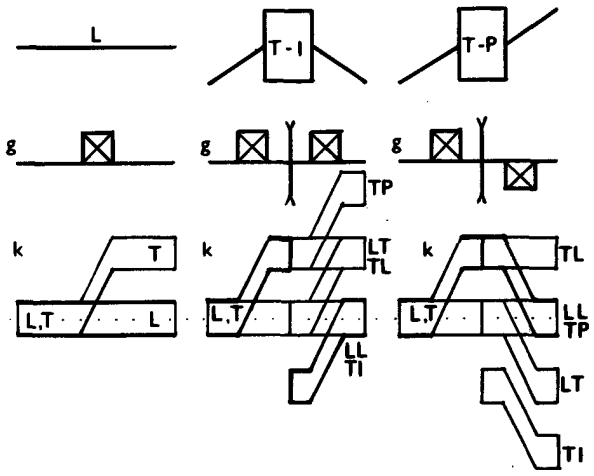

Fig. 3: Gradient-pulse separation schemes extracting the L-pathways (left), the T-I (centre) or the T-P (right) transitions on a compressed pulse. One or two gradient pulses displace the unwanted **k***-trajectories (below) away from the high coherence region.*

	phase trans/rec					selected	
2	T	0	1	.	.		
	R	0	0	.	.	TP,LL,TI	
		0	1	.	.	TL,LT	
3	T	0	2/3	4/3	.		
	R	0	0	0	.	TP,LL	
		0	2/3	4/3	.	LT	
		0	4/3	2/3	.	TL,TI	
4	T	0	1/2	1	3/2		
	R	0	0	0	0	TP,LL	
		0	1/2	1	3/2	LT	&
		0	1	0	1	TI	#
		0	3/2	1	1/2	TL	

Table 1: Phase cycling schemes. Transmitter and receiver phases given as multiples of π. *CYCLOPS and EXORCYCLE are marked by & and #, respectively.*

With frequency selective pulses, the **quality** of selection can be characterized by the rectangularity $\Xi = \Delta_d/\Delta_p$, where Δ_d is the bandwidth of the disturbed region and Δ_p the good quality performance bandwidth.

(A threshold level of 0.025 for deviations from ideality will be used in both cases.) The practical feasibility can be quantified by ratios (4)

$$\eta_m = \max |\gamma B_1(t)| / \Delta_p,$$

$$\eta_E = (\int |\gamma B_1(t)|^2 dt) / \Delta_p,$$

$$\eta_t = T_p . \Delta_p,$$

expressing the relative peak B_1 amplitude, dissipated energy and the pulse length, respectively. Relating these demands to Δ_p is fully justifiable in localized imaging applications, while the average bandwidth $\Delta_s = \Delta_p(1+\Xi)/2$ is more suitable if no space encoding is performed in the direction of selectivity, i.e. in localized spectroscopy, for slice selection etc. The appropriate ratios will be denoted as η_m', η_E' and η_t'.

Concentrating on 90° and 180° pulses with constant gradients, various adiabatic pulses (6,7) have been compared with several types of amplitude- or both amplitude- and phase-modulated selective pulses, symmetric (8), halved (9,10) or unsymmetric (4) in time. Table 2 summarizes the types of pulses compared.

90° pulses	
TR	rectangular
TS n	sinc, n sidelobes (n=7,9)
TG n/q	multiple Gaussian
hRG n/q	halved RG n/q pulses
180° pulses	
RR	rectangular
RS n	sinc, n sidelobes
RG n/q	multiple Gaussian
RAL n/q	AL, linear sweep
RAT n/q	AL, tangential sweep
RAH n/q/λ	AE, hyperbolic secant
RAO n/q	AE, sin/cos
RAS n/q	AE, sin sin/cos sin
AL: adiabatic with linear B_{eff} trajectory	
AE: adiabatic with elliptic B_{eff} trajectory	

Table 2: Types of pulses compared.

Especially the **multiple Gaussian** and the adiabatic pulses deserve a more exact description. In an interval $\langle -T_p/2, T_p/2 \rangle$, the amplitude modulation of the former type (pulses RG n/q, TG n/q) is generally (8)

$$a(t) = \sum_k A_k B_k Q \exp(-\pi B_k^2 Q^2 t^2) . \cos(2\pi B_k C_k Q t),$$

where $Q=q/T_p$ (q=2.5 recommended) is the frequency scale and the parameters A_k, B_k, C_k are given by Table 3.

Pulse	A	B	C	A	B	C
RG 1/q	1	1	0	.	.	.
RG 2/q	1	1	0.5	.	.	.
RG 3/q	1	1	1.5	.770	4.70	0
RG 4/q	1	1	2.3	1.05	4.75	.400
RG 5/q	1	1	2.8	1.21	5.60	.393
				-.12	4.70	0
TG 1/q	1	1	0	.	.	.
TG 2/q	1	1	.45	.	.	.
TG 3/q	1	1	.90	.420	1	0

Table 3: Multiple Gaussian pulses.

The **adiabatic pulses** with linear $B_{eff}(t) = (a(t), 0, \nu + f(t))$ trajectory are characterized by a constant B_1 amplitude a(t)=qF and the frequency sweep linear (11) or tangential (12), i.e.

$$f(t) = 2Ft/T_p$$

or

$$f(t) = qF . \tan(2t/T_p . \arctan(1/q)).$$

The elliptic-type pulses RAH (6) are described by modulation functions

$$a(t) = qF.\mathrm{sech}(\lambda t/T_p),\ f(t) = F.\tanh(\lambda t/T_p),$$

while the RAO (7) and RAS pulses follow the rules of

$$a(t) = qF.\cos\omega(t),\ f(t) = F.\sin\omega(t),$$

with $\omega(t) = \pi t/T_p$ and $\omega(t) = \pi/2\ \sin(\pi t/T_p)$, respectively. The relative length n of all these pulses is given as $n = F.T_p$. Table 4 suggests a suitable choice of values n, q, λ.

RAL	150/0.09		
RAT	150/0.02		
RAH	2/1.3/10	5/1.0/10	8/0.9/10
	10/.8/10	20/.7/10	50/0.47/10
RAO	5/0.6	8/0.5	10/0.53
	20/0.4	50/0.35	
RAS	2/0.87	5/0.8	8/0.8
	10/0.6	20/0.6	50/0.5

Table 4: Adiabatic pulses.

Fig. 4 shows typical sets of transition profiles of the pulses RG and RAH. While no considerable differences in their amplitude profiles can be found, the phase profiles explain the cause of the well-known problems of refocusing adiabatic pulses.

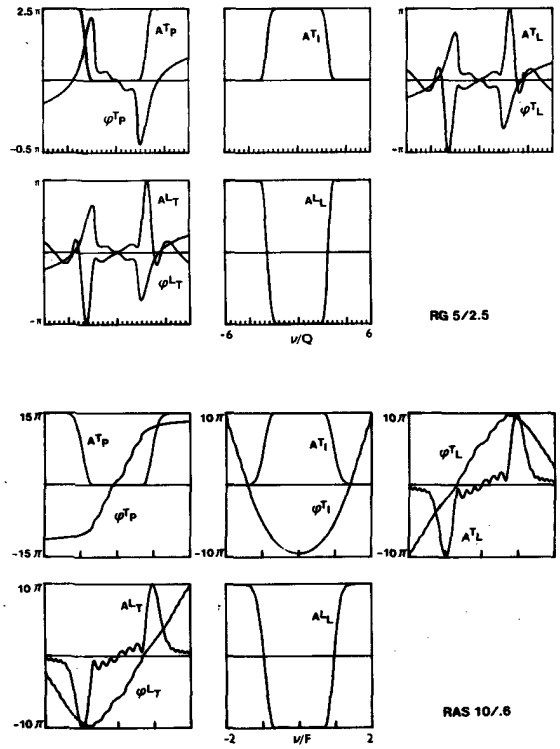

Fig. 4: Complete sets of transition profiles of the RG 5 and the RAS 10 pulses. The amplitude profiles are displayed in the interval <-1,1>.

To demonstrate the application of the transition profiles, the amplitude excitation profiles of various echoes in a CPMG sequence with RG 2/2.5 refocusing pulses are shown in Fig. 5. E.g., the LTI^n pathway is responsible for the n-th refocused echo, the LTLI profile corresponds to the simplest stimulated echo etc.

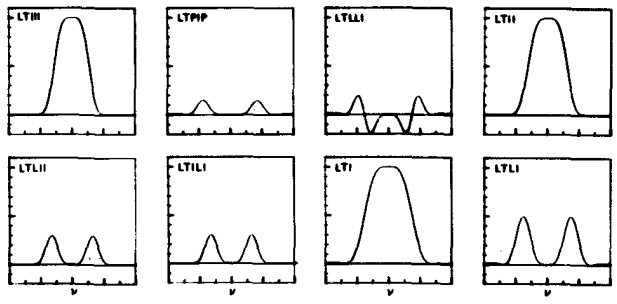

Fig. 5: Excitation profiles of various echoes in a CPMG sequence.

Graphical representation of the relations between selectivity and other properties yields a good survey over the pulse qualities.

Among the **180° pulses** (Fig. 6) the best profile rectangularity can be attained easily with long adiabatic pulses ($\Xi < 1.2$), but good results are also obtained with the multiple Gaussian pulses ($\Xi > 1.3$) or the pulses of Murdoch et al. ($\Xi > 1.5$). Acceleration of the adiabatic passage or reduction of the number of Gaussians lead to profile deterioration. Bad rectangularity characterizes the single Gaussian (RG 1, $\Xi \doteq 20$), the sinc (RS 9, $\Xi \doteq 7$), the tangential-sweep (RAT, $\Xi \doteq 35$) or the rectangular (RR, $\Xi \doteq 70$) pulse.

Even with the same rectangularity, the pulses of different classes may differ considerably in their demands. Especially striking are the differences between the pulses of the best selectivity. The adiabatic pulses are very modest in their B_1 demands, but they must be much longer than other pulses. E.g. comparing the RG, RAH, RAS, and RAO pulses with $\Xi \doteq 1.3$, one finds their relative peak powers 100 : 7.8 : 4.4 : 1.9 and the lengths 1: 3.2 : 6.8 : 8.9, while the dissipated energies (1 : 1.3 : 2.5 : 2.2) do not differ so much. Extremely low B_1 values are sufficient for the RAL pulse, but its length is enormous.

As mentioned above, pulses with different profile rectangularities must be compared considering their application. If selectivity in a direction of localized imaging is supposed, the comparison is to be based on the η_m, η_E, and η_t parameters. It follows from Fig. 6 that lower B_1 field is required for pulses of better selectivity, which can be attributed to the narrower disturbance outside the region of interest. Broadband selective pulses are preferable even for nonselective purposes if their lengths, rapidly increasing with improving the selectivity, are not restrictive. E.g. the pulses from the region of $\Xi \doteq 1.8$ are approximately 30 - 100 times longer than the RR pulse while their peak powers are 10 - 100 times lower. The comparison of energy dissipation reveals a difference between the multiple Gaussian and the adiabatic pulses. While the demands of the former decrease with better selectivity, the latter reach their energy minimum at approximately $\Xi \doteq 1.8$.

The values η_m', η_E', η_t' are important if selectivity in an uncoded direction is considered. In this case an improvement of the profile rectangularity is accompanied by a slight peak power increase with multiple

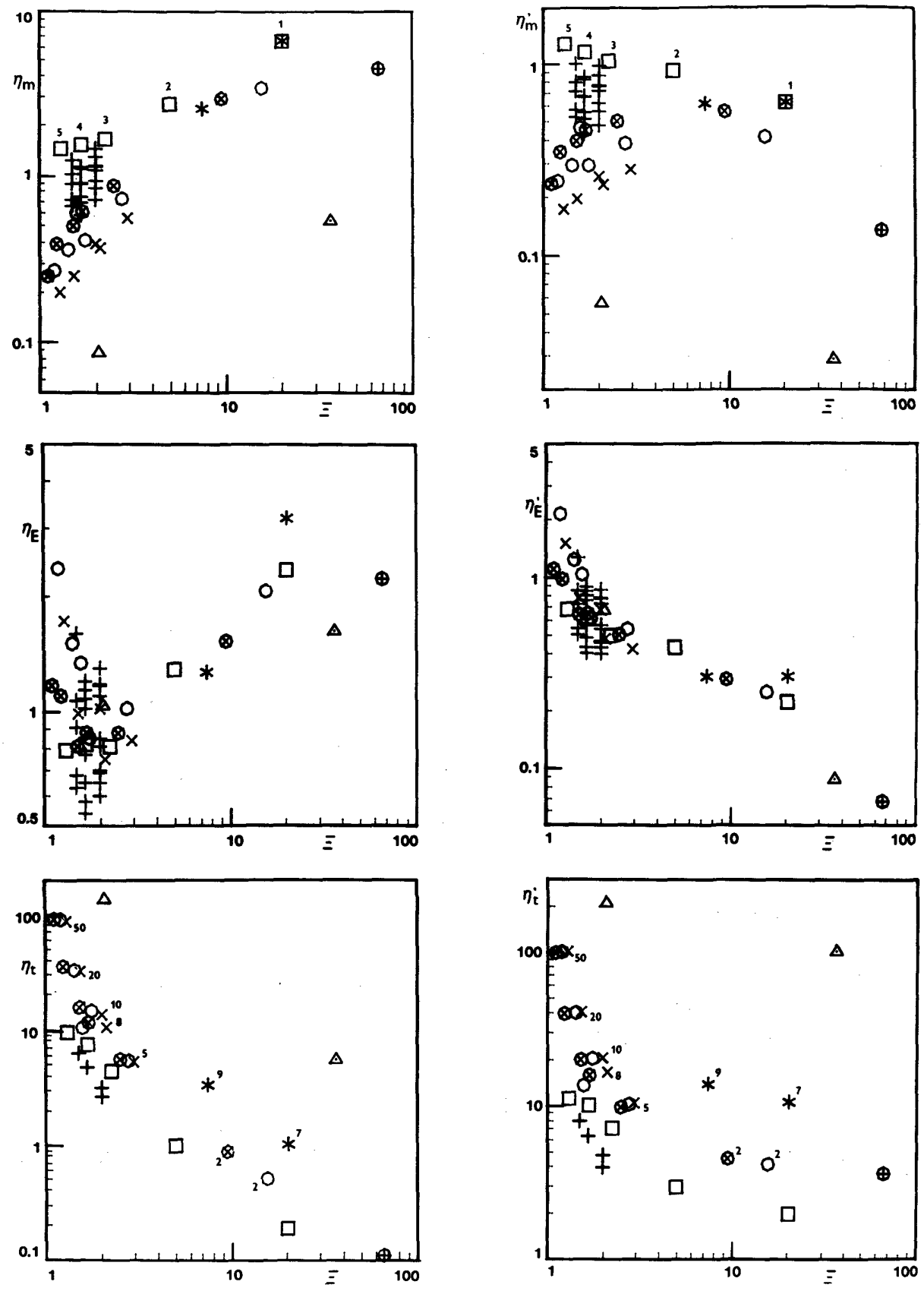

Fig. 6: Comparison of 180° pulses: ⊕ RR, ✱ RS, □ RG, △ RAL, ◬ RAT, ⊗ RAH, × RAO, ○ RAS, + Murdoch et al. (4).

The parameters n (Table 2) are used for identification of pulses.

Gaussian pulses, but a decrease with adiabatic pulses. Unlike the previous case, no general dependence of the necessary peak power on the pulse selectivity is observed. To reach better selectivity, longer pulses are required. The dissipated energy depends practically only on selectivity if $\Xi > 2$, regardless of the pulse. The more selective adiabatic pulses dissipate, however, more energy.

The adiabatic pulses are very suitable for broadband or extremely selective inversions, especially in inhomogeneous excitation fields. On the other hand, multiple Gaussian pulses are appropriate for narrowband inversions in sufficiently homogeneous fields. For refocusing, the phase properties may be of importance.

From the comparison of **90° pulses** (Fig. 7) it follows that the peak power requirements of the hRG pulses are approximately 16 times higher than those of the symmetric TG pulses. Their energy deposition is about 4.4 times higher. Due to the slightly worse selectivity of the halved pulses, they are not much shorter than the symmetric ones.

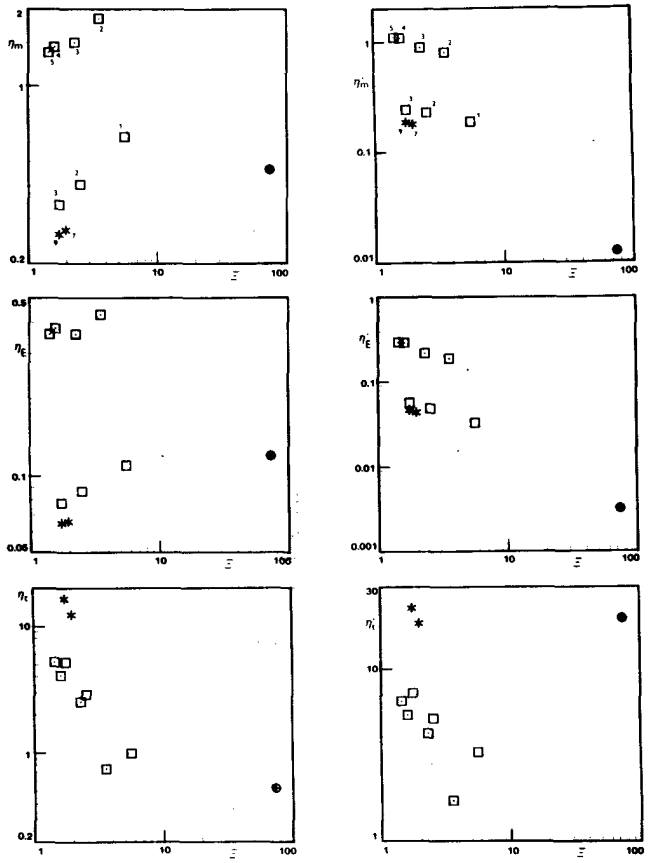

Fig. 7: Comparison of 90° pulses: ⊕ TR, ✳ TS, □ TG, ⊡ hRG.

The comparison shows that better results in one respect are usually compensated by a worse performance in another. To find an optimal pulse, the particular limitations and intentions must be considered to find a reasonable compromise.

References:

1. F. Loaiza, M. A. McCoy, M. H. Levitt, M. S. Silver, W. S. Warren, J. Magn. Reson. 76, 504 (1988)
2. H. Yan, J. C. Gore, J. Magn. Reson. 71, 116 (1987)
3. H. Yan, J. C. Gore, J. Magn. Reson. 75, 427 (1987)
4. J. B. Murdoch, A. H. Lent, M. R. Kritzer, J. Magn. Reson. 74, 226 (1987)
5. R. R. Ernst, G. Bodenhausen, A. Wokaun, "Principles of NMR in One and Two Dimensions", Clarendon Press, Oxford, 1987
6. M. S. Silver, R. I. Joseph, D. I. Hoult, J. Magn. Reson. 59, 347 (1984)
7. K. Uğurbil, M. Garwood, A. R. Rath, M. R. Bendall, J. Magn. Reson. 78, 472 (1988)
8. Z. Starčuk, L. Půček, Z. Starčuk, Jr., J. Magn. Reson. 80, 352 (1988)
9. A. A. Maudsley, J. Magn. Reson. 41, 112 (1980)
10. J. Friedrich, S. Davies, R. Freeman, J. Magn. Reson. 75, 390 (1987)
11. F. Bloch, Phys. Rev. 70, 460 (1946)
12. C. J. Hardy, W. A. Edelstein, D. Valis, J. Magn. Reson. 66, 470 (1986)